33rd Annual International Conference of the IEEE EMBS
Boston, Massachusetts USA, August 30 - September 3, 2011

An Adaptive Algorithm for Real-Time Electrode Calibration

P. Kidmose

Abstract— **Continuous brain monitoring based on EEG recorded from surface electrodes is believed to have potentials in wearable medical devices. In such devices capacitive electrodes are attractive compared to conventional electrodes because there is no need for skin preparation and conductive gels, and because of diminished motion artifacts. However, there are technical challenges connected to the practical application of capacitive electrodes. The electrode capacitance, which has significant impact on the signal measured, will vary between channels and will be time varying. Therefore calibration of the electrode array is an important preprocessing step before the signal processing. This paper proposes an algorithm for blindly estimating the parameters of the analog signal acquisition paths, including the capacitances of the electrodes. The algorithm continuously estimates the parameters, based on the measured EEG signals, and compensates for variations in the analog signal paths. Simulations show that the algorithm can estimate the parameters, and track changes of the electrodes capacitance in real-time.**

I. Introduction

Electroencephalography (EEG) recordings provide a non-invasive way to monitor neural activity in the human brain at temporal and spatial scales of interest in various applications ranging from medical devices to brain computer interfaces (BCI) [1].

Continuous brain monitoring based on EEG is envisaged to become a part of everyday life in wearable medical devices. Such devices have applications within diagnosis and monitoring of disease progression, for therapy evaluation and rehabilitation for neurodegenerative diseases, psychiatric disorders [2], and sleep disorders; and for warning and monitoring of seizures for e.g. epilepsy[3] and hypoglycemia[4].

Conventional EEG recordings are based on electrodes that have galvanic connection to the body. Whether the electrode is close to the ideal non-polarizable or ideal polarizable electrode a half cell potential will arise in the interface between the metallic electrode and the human body. This half cell potential is the origin of the so called *motion artifacts* which is a serious cause of interference when measuring bioelectrical potentials [5].

As an alternative to the conventional electrodes are capacitive electrodes that measure the bioelectrial potential through a capacitive interface to the body relying solely on displacement currents in the electrode interface. In capacitive electrodes no half cell potential arises and therefore no motion artifacts are generated. Early work on capacitive electrodes for ECG and EMG recordings are reported in [6] and [7]; more recently [8] describes the build of an amplifier circuit for bioelectrical potential recordings and in [9] and [10] it is demonstrated that this can be used for EEG recordings.

Capacitive electrodes provide some important advantages over conventional electrodes that makes the use of capacitive electrodes attractive for applications within the field of the before mentioned wearable devices:

- Contrary to conventional electrodes capacitive electrodes does not require conductive gel and skin preparation. Thus capacitive electrodes may result in devices that are easier to handle and to put in place, and more comfortable to use.
- Capacitive electrodes do not have a metal-electrolyte interface and hence no half cell potentials. Therefore, contrary to conventional electrodes, capacitive electrodes do not have motion artifacts.

On the other hand there are technical challenges related to capacitive electrodes that have to be addressed. For realistic electrode sizes the electrode capacitance is very small resulting in very high input impedance requirement for the front-end amplifier circuitry. This imposes challenges and trade offs with respect to noise and ESD protection. Furthermore the transfer function, from potentials generated by currents related to neural activity to the output of the instrumentation equipment, depends on the electrode capacitance.

In practical systems the electrode capacitance will be subject to considerable uncertainties, will vary between channels and will be time varying; thus having significant impact on the acquired signals. Therefore calibration of the electrode array is an important preprocessing step. Further, it is of crucial importance in medical devices to be able to validate if there is sufficient electrode capacitance to rely on the acquired signals and act if this is not the case.

This paper presents an algorithm for real-time calibration of the signal acquisition paths for use in devices that measure bioelectrical potentials using a capacitive electrode instrumentation. In Section II a typical instrumentation amplifier setup is analyzed, a discrete time model is established and the input related noise sources are quantified. In Section III an algorithm for estimating the parameters of the analog signal paths is developed; and in Section IV a simulation example demonstrates that the algorithm can estimate the parameters of the analog signal paths and can track time varying poles induced by e.g. electrodes movements.

II. Signal Path Model and Noise Analysis

For the purpose of the following analysis an electrical diagram of a practical instrumentation for capacitive measurement of EEG signals is shown in Fig. 1. The electrodes are modeled as ideal capacitors and are denoted C_{E1} and

P.Kidmose (pki@iha.dk) is with Engineering College of Aarhus / Aarhus School of Engineering, Aarhus University, 8000 Aarhus C, Denmark

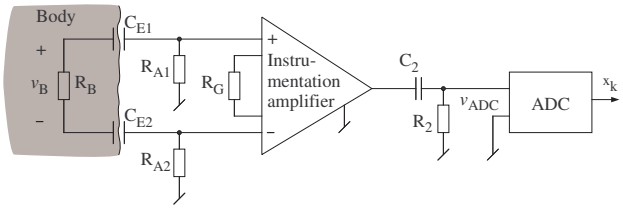

Fig. 1. Electrical diagram of a practical instrumentation for capacitive measurement of EEG signals.

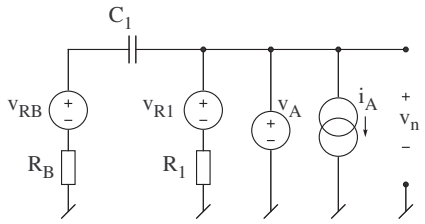

Fig. 2. Electrical equivalent diagram for analysis of input related noise of the instrumentation amplifier. V_{RB} and V_{R1} is the thermal noise related to R_B and R_1 respectively. V_A is the voltage noise and I_A is the current noise of the instrumentation amplifier.

C_{E2}. The DC bias current return path resistors are denoted R_{A1} and R_{A2}, and the tissue impedance from electrode to electrode is denoted R_B. The gain of the instrumentation amplifier is set by R_G. A suitable instrumentation amplifier for this purpose could be the INA116 from TI, see [11].

The continuous time transfer function, from the electrode differential signal to the input of the analog-digital converter (ADC), for the instrumentation depicted in Fig.1 is

$$H(s) = \frac{v_{\text{ADC}}}{v_{\text{B}}} = \left(1 + \frac{R_I}{R_G}\right) \frac{R_1 C_1 s}{R_1 C_1 s + 1} \frac{R_2 C_2 s}{R_2 C_2 s + 1} \quad (1)$$

where $R_1 = R_{A1} + R_{A2}$, $C_1 = C_{E1} \cdot C_{E2}/(C_{E1} + C_{E2})$ and R_I is an integrated part of the instrumentation amplifier. For the purpose of the parameter estimation algorithm developed in Section III the corresponding discrete time model is obtained using the matched pole-zero method

$$H(z) = K \frac{1 + z^{-1}}{1 + a_1 z^{-1}} \frac{1 + z^{-1}}{1 + a_2 z^{-1}} \quad (2)$$

where a_1 and a_2 are related to the continuous time poles $s = -1/R_1C_1$ and $-1/R_2C_2$ respectively, and K is related to the overall gain determined by R_G and R_I.

Capacitive electrodes with realistic electrode area will typically have capacitance, within an order of magnitude, of 10 pF. Choosing the DC bias current return path resistors, R_{A1} and R_{A2}, to 50 GΩ, and assuming 10 pF capacitance for each electrode, yields a cut off frequency of 1.27 Hz.

The signal acquisition performance of such an instrumentation is limited by noise. Because of this, and because the noise floor will have impact on the performance of the parameter estimation algorithm developed in the next section, it is appropriate to make a noise analysis. An electrical equivalent diagram, for the instrumentation amplifier part of the diagram in Fig.1, is shown in Fig. 2. The power spectral density of the thermal noise of the resistors is given by $v^2 = 4k_BTR$, where k_B is Boltzmann's constant (J/K), T is the resistor's absolute temperature (K), and R is the resistor value (Ω). At 20°C this gives $v_n = 0.127\text{nV}\sqrt{R}/\sqrt{Hz}$; thus the bias current return path resistors result in a thermal noise generator of 20.1 $\mu\text{V}/\sqrt{\text{Hz}}$.

To illuminate the electrode capacitance influence on the noise, the input related noise spectra for the 4 different noise source are shown in Fig.3, and the spectra are shown for C_1 = 5 pF (solid line) and 25 pF (dashed line). Further, it is readily seen that the electrode capacitance influences the low frequency shaping of the bioelectrical source signal[1].

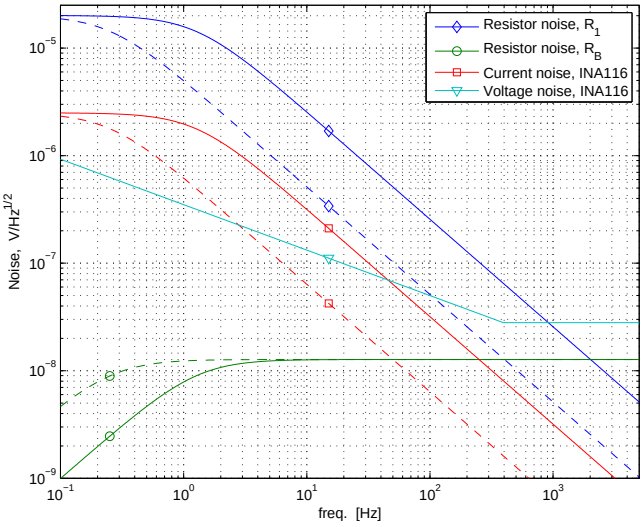

Fig. 3. Input related noise spectra for the 4 different noise sources. The spectra are shown for C_1 = 5 pF (solid line) and C_1 = 25 pF (dashed line). Current noise and voltage noise values are taken from [11].

III. Electrode Calibration Algorithm

The purpose of the electrode calibration algorithm is to compensate for gain and frequency shaping differences between the different analog signal paths. This is obtained by estimating the parameters in the transfer function in Eq. 2 for each signal path, and filtering with the inverse of this transfer function. The parameter estimation is inherently a blind problem since the source signal is unknown, and only a filtered version of the source signal is observable. However, it is possible to estimate the parameters based on the assumption that the long term power spectral density of the electrode potential is similar in between channels.

As explained later, the power spectral density must be estimated at several frequency points in the frequency range where the poles of the analog signal paths are located. For

[1]Put to the authors attention by one of the reviewer [12] provides an excellent review of biopotential front ends, and there there is a more thorough analysis of such front end circuitry.

the instrumentation considered here this will be at very low frequencies (delta band). The application that is in mind for this algorithm is for electrode arrays with small electrode distances. Since the EEG signals reflect aggregated electrical activity from highly spatially distributed neural sources, and because of the small electrode distances, the assumption about the similarity of the power spectral density is expected to be realistic. However, the assumption must be supported by EEG measurements.

The power spectrum of the source signal, s_k, for the kth channel is denoted $P_{s_k}(\omega) = S_k^*(\omega) \cdot S_k(\omega)$, where $S_k(\omega)$ is the fourier transform of s_k and * denotes complex conjugated. The power spectrum of the measured signal, x_k, is then

$$P_{x_k}(\omega) = P_{s_k}(\omega) \cdot H_k^*(\omega) \cdot H_k(\omega) = P_{s_k}(\omega) P_{h_k}(\omega) \quad (3)$$

where $H_k(\omega)$ is the transfer function for the kth channel. By insertion of the parameterized transfer function from Eq.2 the power spectrum, $P_{h_k}(\omega)$, is

$$\begin{aligned} P_{h_k}(\omega) &= K_k^2 \frac{1+e^{j\omega}}{1+a_{1k}e^{j\omega}} \frac{1+e^{-j\omega}}{1+a_{1k}e^{-j\omega}} \\ &\quad \frac{1+e^{j\omega}}{1+a_{2k}e^{j\omega}} \frac{1+e^{-j\omega}}{1+a_{2k}e^{-j\omega}} \\ &= K_k^2 \frac{2(1+\cos(\omega))}{1+2a_{1k}\cos(\omega)+a_{1k}^2} \\ &\quad \frac{2(1+\cos(\omega))}{1+2a_{2k}\cos(\omega)+a_{2k}^2} \end{aligned} \quad (4)$$

Now let $G_{x_k}(\omega)$ denote the power spectrum estimated from the observed discrete time signal, x_k, from the kth channel. A cost-function, that measures the difference between the observed power spectrum ratio and the parameterized power spectrum ratio, for a system comprising M channels and evaluated in N frequency points is

$$Q = \frac{1}{2}\sum_{n=1}^{N}\sum_{k=1}^{M-1}\sum_{m=k+1}^{M}\left(\frac{G_{x_k}(\omega_n)}{G_{x_m}(\omega_n)} - \frac{P_{x_k}(\omega_n)}{P_{x_m}(\omega_n)}\right)^2 \quad (5)$$

If we assume that the source signals power spectrum are identical, i.e. $P_{s_k}(\omega) = P_{s_m}(\omega)$, the cost function simplifies to

$$Q_s = \frac{1}{2}\sum_{n=1}^{N}\sum_{k=1}^{M-1}\sum_{m=k+1}^{M}\left(\frac{G_{x_k}(\omega_n)}{G_{x_m}(\omega_n)} - \frac{P_{h_k}(\omega_n)}{P_{h_m}(\omega_n)}\right)^2 \quad (6)$$

where $P_{h_k}(\omega)$ is the power spectrum for the kth channel parameterized as shown in Eq. 4. The assumption may seem very restricting, but as long as there is no systematic difference between the power spectra densities, it will have only minor influence on the minimum for the cost function. Choosing the number of frequency points, N, larger than the number of parameters to be estimated, will in general reduce the impact from deviations from the assumption.

The parameter estimates, needed for calibration, are obtained by minimizing the cost function in Eq.6 with respect to the parameters. This is a non-linear least squares problem for which numerous numerical solving methods exist.

Next, without loss of generality, an algorithm for a 2-channel system is developed. For $M = 2$ the cost function in Eq.6 can then be written as

$$\begin{aligned} Q_2 &= \frac{1}{2}\sum_{n=1}^{N}\left(\frac{G_{x_1}(\omega_n)}{G_{x_2}(\omega_n)} - \frac{P_{h_1}(\omega_n)}{P_{h_2}(\omega_n)}\right)^2 \\ &= \frac{1}{2}\mathbf{e}^T \cdot \mathbf{e} \end{aligned} \quad (7)$$

where

$$\mathbf{e} = [e(\omega_1)\ \ e(\omega_2)\ \ \ldots\ \ e(\omega_N)]^T$$

and

$$e(\omega_n) = \frac{G_{x_1}(\omega_n)}{G_{x_2}(\omega_n)} - \frac{P_{h_1}(\omega_n)}{P_{h_2}(\omega_n)}$$

Whether a simple steepest descent type of algorithm or more advanced hybrid algorithms, combining the Gauss-Newton and the steepest descent direction, is applied, we must calculate the Jacobian matrix

$$\mathbf{J} = \frac{\partial \mathbf{e}^T}{\partial \boldsymbol{\theta}} \quad (8)$$

where $\boldsymbol{\theta} = [a_{11}\ \ a_{12}\ \ a_{21}\ \ a_{22}\ \ K]^T$ is the parameter vector. The parameters (a_{11}, a_{12}) and (a_{21}, a_{22}) are the parameters associated with channel 1 and 2 respectively; and K is the gain ratio K_1/K_2. Notice that because of the blind nature of the algorithm there is a gain uncertainty, and therefore only the ratio between channel gains can be estimated.

For the 2 channel algorithm outlined here the elements of the nth column of the $\mathbb{R}^{5\times N}$ Jacobian matrix is

$$\begin{aligned} J_{1n} &= d_{11}'(\omega_n)K^2\frac{d_{21}(\omega_n)}{d_{11}(\omega_n)^2}\frac{d_{22}(\omega_n)}{d_{12}(\omega_n)} \\ J_{2n} &= d_{12}'(\omega_n)K^2\frac{d_{21}(\omega_n)}{d_{11}(\omega_n)}\frac{d_{22}(\omega_n)}{d_{12}(\omega_n)^2} \\ J_{3n} &= -K^2\frac{d_{21}'(\omega_n)}{d_{11}(\omega_n)}\frac{d_{22}(\omega_n)}{d_{12}(\omega_n)} \\ J_{4n} &= -K^2\frac{d_{21}(\omega_n)}{d_{11}(\omega_n)}\frac{d_{22}'(\omega_n)}{d_{12}(\omega_n)} \\ J_{5n} &= -2K\frac{d_{21}(\omega_n)}{d_{11}(\omega_n)}\frac{d_{22}(\omega_n)}{d_{12}(\omega_n)} \end{aligned}$$

where

$$\begin{aligned} d_{11}(\omega_n) &= 1+2a_{11}\cos(\omega_n)+a_{11}^2 \\ d_{12}(\omega_n) &= 1+2a_{12}\cos(\omega_n)+a_{12}^2 \\ d_{21}(\omega_n) &= 1+2a_{21}\cos(\omega_n)+a_{21}^2 \\ d_{22}(\omega_n) &= 1+2a_{22}\cos(\omega_n)+a_{22}^2 \end{aligned}$$

and

$$\begin{aligned} d_{11}'(\omega_n) &= \frac{\partial}{\partial a_{11}}d_{11}(\omega_n) = 2(\cos(\omega_n)+a_{11}) \\ d_{12}'(\omega_n) &= \frac{\partial}{\partial a_{12}}d_{12}(\omega_n) = 2(\cos(\omega_n)+a_{12}) \\ d_{21}'(\omega_n) &= \frac{\partial}{\partial a_{21}}d_{21}(\omega_n) = 2(\cos(\omega_n)+a_{21}) \\ d_{22}'(\omega_n) &= \frac{\partial}{\partial a_{22}}d_{22}(\omega_n) = 2(\cos(\omega_n)+a_{22}) \end{aligned}$$

The parameter estimation is based on power spectrum estimates of the observed signals. To have a determined set of equations the number of frequency points, in which the power spectra are estimated, must at least equal the number of parameters that are to be estimated. Furthermore, to obtain a well-conditioned Jacobian matrix, the frequency points must be chosen to be in the frequency range where the poles of the system are.

IV. Simulation Example

In the following simulation example a simple version of the Marquardt algorithm is used with the update equation

$$\boldsymbol{\theta}_p = \boldsymbol{\theta}_{p-1} - (\mathbf{J}\mathbf{J}^T + \mu\mathbf{I})^{-1}\mathbf{J}\mathbf{e} \tag{9}$$

The subscripted p denotes the iteration number, and the adaptation constant μ is set to 1.0.

The analog signal paths, for which the parameters are to be estimated, is a 2-channel system with 5 parameters as outlined in the previous section. The parameter estimation is based on power spectrum values in 10 frequency points logarithmic distributed between 0.1 Hz and 10 Hz. It is assumed that the observed power spectra, G_{x_1} and G_{x_2}, are known; while in a real world embodiment these must be estimated from the observed signals, x_1 and x_2, using e.g. an FFT based algorithm.

The simulation example shows that, given the true power spectra estimates, the algorithm will converge fast towards the true parameter values. In this specific specific simulation the 4 analog poles are located at 5.0, 0.30, 2.5 and 1.6 Hz, and the gain ratio is 1.2. In the top panel of Fig.4 the trajectory of the parameters versus the iteration number is shown. The solid lines show the parameter convergence towards the optimal parameter values which are shown as dashed lines. In the bottom panel the cost function, Q_2, versus iteration number is shown.

Other simulations have shown, which is also supported by the convergenge behavior in Fig.4, that the algorithm tracks changes in the parameters very smoothly.

In a real world implementation caution must be taken when estimating the power spectra. It is observed from Fig. 3 that the current noise from the instrumentation amplifier and the thermal noise contribution from R_1 is not shaped by the $s = -1/R_1C_1$ pole. Thus, reliable power spectra estimates can only be obtained if the levels of the signals are significantly higher than the noise floor generated by these noise sources.

V. Conclusion

This work proposes a blind adaptive algorithm for real-time electrode calibration in multiple channel systems. Simulations show that the algorithm can estimate the parameters related to the analog signal path, and that it can track changes in these parameters. These characteristics are important in real world wearable devices, because the parameters of the analog signal paths are unknown and time varying, and therefore must be estimated in order to calibrate the electrode system.

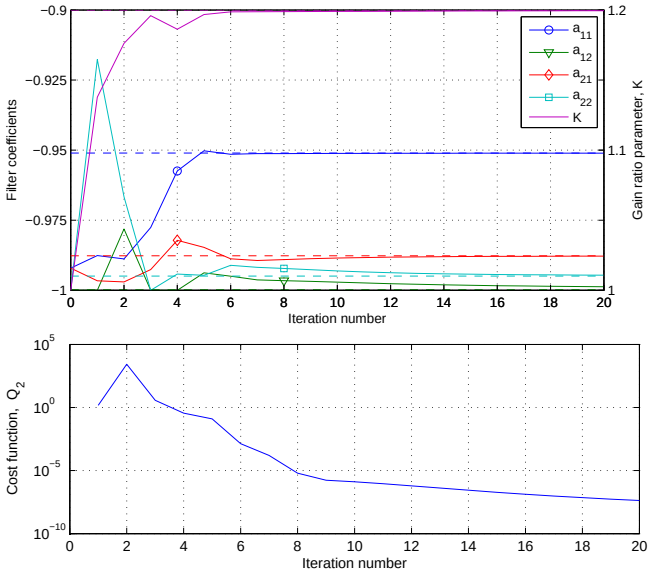

Fig. 4. **Top panel** Trajectory of the parameters versus the iteration number. The solid lines show the parameter convergence towards the optimal parameter values shown as dashed lines. The right hand side axis is for the filter coefficients, a_{11},a_{12}, a_{21} and a_{22}; and the left hand side axis is for the gain ratio parameter, K. **Bottom panel** Cost function versus iteration number showing the convergence of the algorithm

References

[1] J.R.Wolpaw, N.Birbaumer, D.J.McFarlanda, G.Pfurtschellere, and T.M.Vaughana, "Braincomputer interfaces for communication and control," *Clinical Neurophysiology*, vol. 113, no. 6, 2002.

[2] A.Khodayari-Rostamabad, J.P. Reilly, G.Haseyand H. de Bruin, and D. MacCrimmon, "Using pre-treatment EEG data to predict response to SSRI treatment for MDD," *Engineering in Medicine and Biology Society*, pp. 6103–6106, August 2010.

[3] K.K.Jerger, T.I.Netoff, J.T.Francis, T.Sauer, L.Pecora, S.L.Weinstein, and S.J.Schiff, "Early Seizure Detection," *Journal of Clinical Neurophysiology*, vol. 18, no. 3, pp. 259–268, May 2001.

[4] J.Gade, A.Rosenfalck, and I.Bendtson, "Detection of EEG Patterns Related to Nocturnal Hypoglycemia," *Methods of Information in Medicine*, vol. 33, pp. 153–156, 1994.

[5] John G. Webster, *Medical instrumentation: application and design*, John Wiley & Sons, 2010.

[6] A.Lopez and P.C.Richardson, "Capacitive Electrocardiographic and Bioelectric Electrodes," *IEEE Transactions on Bio-medical Engineering*, vol. 16, pp. 99, January 1969, Short Communications.

[7] A.Potter and L.Menke, "Capacitve Type of Biomedical Electrode," *IEEE Transactions on Bio-medical Engineering*, pp. 350–351, October 1970, Short Communications.

[8] R.J.Prance, A.Debray, T.D.Clark, H.Prance, M.Nock, C.J.Harland, and A.J.Clippingdale, "An Ultra-low-noise Electrical-potential probe for Human-body Scanning," *Measurement Science and Technology*, vol. 11, no. 3, pp. 291–297, March 2000.

[9] R.J.Prance, S.Beardsmore-Rust, A.Aydin, C.J.Harland, and H.Prance, "Biological and Medical Applications of a new Electric Field Sensor," *ESA Annual Meeting on Electrostatics*, 2008.

[10] C.J.Harland, T.D.Clark, and R.J.Prance, "Remote Detection of Human Electroencephalograms using Ultrahigh Input Impedance Electric Potential Sensors," *Applied Physics Letters*, vol. 81, no. 17, pp. 3284–3286, October 2002.

[11] Burr-Brown Corporation, "Instrumentation Amplifier INA166. Ultra Low Input Bias Current Instrumentation Amplifier.," http://focus.ti.com/docs/prod/folders/print/ina116.html.

[12] Enrique Spinelli and Marcelo Haberman, "Insulating electrodes: a review on biopotential front ends for dielectric skinelectrode interfaces," *Physiological Measurement*, vol. 31, pp. 183–198, 2010.